Femtosecond laser driven high-flux highly collimated MeV-proton beam

著者	Nishiuchi M., Daido H., Yogo A., Orimo S., Ogura K., Ma J., Sagisaka A., Mori M., Pirozhkova A. S., Kiriyama H., Bulanov S. V., Esirkepov T. Zh., Choi Il Woo, Yu Tae Jun, Shung Jae Hee, Jeong Tae Moon, Kim Hyung Taek, Hong Kyung-Ham, Noh Young-Chul, Ko Do-Kyeong, Lee Jongmin, Oishi Y., Nemoto K., Nagatomo H., Nagai Keiji
著者別表示	長井 圭治
journal or publication title	AIP Conference Proceedings
volume	1024
page range	137-150
year	2008-06-30
URL	http://doi.org/10.24517/00067088

doi: 10.1063/1.2958186

Femtosecond laser driven high-flux highly collimated MeV-proton beam

Cite as: AIP Conference Proceedings **1024**, 137 (2008); https://doi.org/10.1063/1.2958186
Published Online: 30 June 2008

M. Nishiuchi, H. Daido, A. Yogo, et al.

Femtosecond laser driven high-flux highly collimated MeV-proton beam

M. Nishiuchi,[1],* H. Daido,[1] A. Yogo,[1] S. Orimo,[1] K. Ogura,[1] J. Ma,[1] A. Sagisaka,[1] M. Mori,[1] A. S. Pirozhkov,[1] H. Kiriyama,[1] S. V. Bulanov,[1,2] T. Zh. Esirkepov,[1]

1Advanced Photon Research Center,
Kansai Research Establishment, Japan Atomic Energy Agency,
8-1 Umemi-dai, Kizu, Kyoto 619-0215, Japan
2A.M.Prokhorov Institute of Russian Academy of Sciences,
Vavilov St. 38, Moscow 119991, Russia

Il Woo Choi,[3] Tae Jun Yu,[3] Jae Hee Shung,[3] Tae Moon Jeong,[3] Hyung Taek Kim,[5] Kyung-Ham Hong,[5] Young-Chul Noh,[5] Do-Kyeong Ko,[3] and Jongmin Lee[3]

3 Advanced Photonics Research Institute,
Gwangju Institute of Science and Technology, Korea

Y. Oishi,[4] K. Nemoto,[4]

4Central Research Institute of Electronic Power Industry

H. Nagatomo,[5] K. Nagai,[5]

5nstitute of Laser Engeneering, Osaka University, Osaka 565-0871, Japan
(Dated: November 20, 2007)

Abstract. Highlly collimated energetic protons whose energies are up to 4MeV are generated by an intense femtosecond Titanium Sappheire laser pulse interacting with a 7.5, 12.5, and 25μm-thick Polyimide tape target and 5μm-thick copper target. We find no clear difference on the proton spectra from 7.5, 12.5, and 25μm Polyimide tape target. The highest conversion efficiency from laser energy into protons of ~3% is observed with a 7.5μm thick Polyimide target. The quality of the proton beam is good enough to obtain a clear projection image of a mesh having 10μm line and space structure, installed into the passage of the beam. We obtain clear vertical lines on the proton intensity profiles from the copper target, which are considered to be transferred from the surface of the copper target. From it, we can restrict the size of the proton emitting region to be ~20μm.

PACS numbers: 52.38.Kd, 52.50.Jm, 52.59.-f

CP1024, *Laser-Driven Relativistic Plasmas Applied for Science, Industry, and Medicine - The 1st International Symposium*
edited by S. V. Bulanov and H. Daido

INTRODUCTION

We have observed significant progress on the generation of fast protons from the interaction between a short-pulse-intense laser and a thin foil target (see review articles [1, 2]). Those fast protons generated from a laser-driven plasma have significant features. Among them, the most unique one is that more than 10^{11} protons are emitted from the source having a size of ~10μm, within a time-scale of ~1 ps at a source [3-5]. Such an intense beam has never been achieved by conventional accelerators. The laser-driven proton beams have extremely low transeverse emittance, compared with those of the beams from conventional accelerators [3-5]. The proton beams have quite large divergence angle of >10~20° at Full Width at Half Maximum (FWHM). The energy spectra of those protons exhibit wide energy spread. Because of such peculiar features, the proton beams from a laser-driven plasma have great potentiality as to be used in many applications. For example, such a proton source is applicable to an injector for a conventional accelerator [6], a table-top stand-alone accelerator of charged particles [7, 8], and high-resolution proton radiography system[9]. They are also applicable to the field of material science [10] and the production of short-lived isotopes for medical and industrial applications [11, 12].

However, for the practical use of the proton beams in specific fields, we have to overcome important issues, such as the extension of the maximum energy of the protons and the improvement of the conversion efficiency of the laser energy into kinetic energy of the protons. In addition to that, we have to deliver the proton beams repetitevely and stably for the applications.

By the laser-driven ponderomotive force, the electrons are accelerated upto the relativistic speed. Those electrons penetrate the target from front to rear surfaces and form quasi-static electric field at the rear surface. Ions from the contaminant layer at the surface of the taget are then accelerated by this acceleration field [13].

The maximum energy of protons obtained with the laser-plasma interaction so far is 58 MeV by using the combination of single shot base Peta-watt laser system [13-15]. In this experiment, CH targets with thickness of 70μm were used. The conversion efficiency of the laser energy into those of protons (with the energy range of E>10 MeV) was 12%. Total laser energy of ~400 J is concentrated within 500 fs duration to achieve such high maximum energy of protons and conversion efficiency.

After the proof of principle studies, systematic studies have been extensively carried out experimentally for obtaining higher energy as well as higher intensity protons by changing experimental parameters, such as target material, target thickness, laser intensity, laser energy, laser duration, pre-pulse conditions, and so on. Among these parameters, duration and intensity of prepulse due to the amplified spontaneouse emission (ASE) play an important role.

It is strongly desired that the density gradient at the target rear surface should remain steep for obtaining higher energy protons as well as higher conversion efficiency. Theoretical studies also predict that the proton acceleration could be more efficient by using extremely thin targets [20, 21]. It is shown experimentally that proton energy could be increased by decreasing the target thicknesses [16, 19]. However, when the intensity of the laser increases, the leading edge or the pedestal caused by an ASE also increases to reach the level of 10^{12} Wcm^{-2}, at which level, a

shock wave propagates through the target from front to rear surfaces. The shock destroys the steepness of the density gradient at the rear surface of the target or even disassembles the target itself at the time of the main pulse arrival.

Mackinnon et al. [16] have obtained protons with a maximum energy of 25 MeV. In order to decrease the pre-pulse intensity, the second harmonics of the Ti:sapphire laser was used. An Al target with the thickness of 3μm was used. The total laser energy is ~1 J and the pulse width is 100 fs with sharp pulse rize time of ~10 fs. However, the conversion efficiency remained ~1% for the protons within total energy band.

In order to use thinner target, plasma mirrors and fast Pockels cells were used to decrease the ASE level and adjust the duration of the ASE [24, 25]. Antici et al. [25] have obtained maximum proton energy of ~7.3 MeV and energy conversion efficiency of ~4% (protons with the energies of E>1.8 MeV) by applying the laser pulse, whose energy, duration and the ASE level of 1 J, 320 fs, and ~10^{-10}, onto an extremely thin, such as, 30 nm thick SiN planar membranes target. They used double plasma mirrors to realize the higher contrast of the laser pulses. It is by far the highest energy conversion efficiency from laser to kinetic energies of protons obtained with a ~100 TW-class laser system.

In order to apply the proton beam from a laser driven plasma for many applications, it is desired to obtain proton beams with higher energies and higher energy conversion efficiencies by repetitive operations. In this paper, we report on experiments performed to obtain the proton beams with high energy conversion efficiency of up to ~3% (to the protons with the energies of >0.8 MeV) with the maximum energy of 4 MeV. We realize repetitive production of a proton beam with such a high conversion efficiency with simplified system, such as the combination of a 100 TW class laser system and the tape target system. We use relatively thick target, such as, 7.5, 12.5, and 25μm-Polyimide target as well as 5μm -copper target, instead of very thin target. The tape target system realizes the repetitive supply of the fresh surface to the focal spot [17].

EXPERIMENTAL SETUP

The experiment is carried out at Advanced Photonics Research Institute, Gwangju Institute of Science and Technology (GIST), Korea. The experimental setup is shown in Fig.1. A Ti:Sapphire laser system delivers p-polarized pulses, whose energies and pulse durations on taget are 1.7 J and 35 fs, respectively. A central wavelength is 800 nm. The laser pulses are focused onto the target with an F/3.3 off-axis parabolic mirror (OAP) with an incident angle of 45°. About ~63% of the laser energy is contained within a $1/e^2$ focal spot of ~9μm. The resultant laser intensity at the focal spot is ~3×10^{19} Wcm^{-2}. Polyimide [$(C_{16}H_6O_4N_2)_n$] targets with the thickness of 7.5, 12.5, and 25μm are used. A fresh surface of the target is delivered to the focal spot at each shot by the tape target driver [17]. The position of the target in the target normal direction

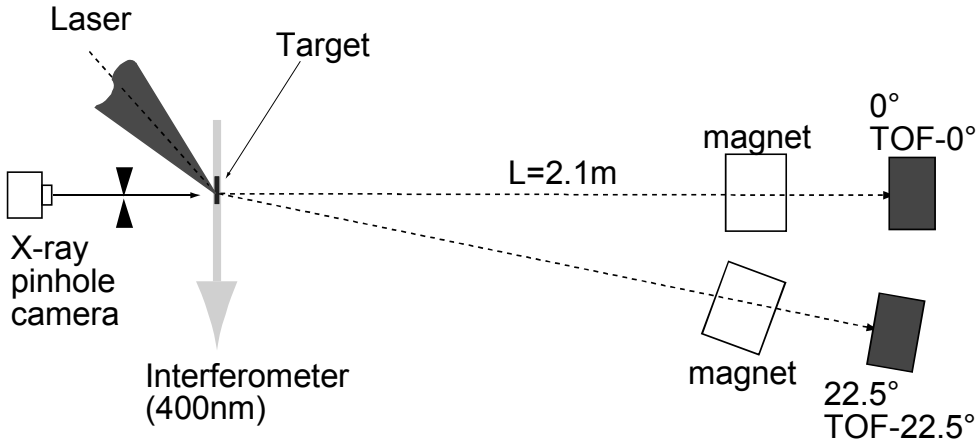

FIGURE 1. Experimental setup. "TOF" stands for time of flight proton energy spectrometer. TOF-0°and TOF-22.5° represent one which is placed normal to the target rear surface and at 22.5°from the normal.

is monitored by the X-ray pinhole camera which delivers us an X-ray image of theplasma on the target surface in ~keV region. The target is placed always within ±10μm from the 1st shooting point in the target normal direction, which is sufficiently smaller than the Rayleigh length of the parabolic mirror of ~200μm.

The contrast ratio of ASE-pedestals are 1×10^{-10} before the Pockels cell switching time and 4×10^{-8} after the Pockesl cell switching time before the main pulse respectively. The duration of the ASE-pedestal is controlled by adjusting timing of Pockels cell to be 1.5 ns or 3 ns. A pre-plasma which is generated by the interaction between a pre-pulse as well as an ASE-pedestal and the target before the arrival of the main pulse is monitord by an interferometer system using a 800 nm wavelength beam [18]. The probe pulse of the interferometer system probes pre-plasma 50 ps before the main pulse arrival. Protons are measured by the online time-of-flight (TOF) spectrometers [22] which are placed at the target rear side. One of them is placed at target normal direction (hereafter TOF-0°) and the other is at the angle of 22.5° (hereafter TOF-22.5°) with respect to the laser propagation direction. Each TOF spectrometer consists of a plastic scintillator whose thicknesses are 0.5 mm and 0.2 mm for TOF-0° and TOF-22.5°, respectively. The scintillators are covered with Al filters whose thicknesses are 2 μm for both TOF spectrometers in order to reject the contamination of the laser light into the signal. As a result, protons whose energies are between ~300 keV and 6 MeV are detected with TOF-0° and ~300 keV and 4 MeV with TOF-22.5°. The TOF-0° has an aperture of 35 mm in diameter and the TOF-22.5° has an apeture of 42 mm in diameter. Protons are detected at the above scintillators after passing through the flight distance of L=2.1 m. Dipole magnets are installed onto the passage of the protons in order to reject the electrons from the plasma to be detected on the scintillators. The magnetic field provided from this dipole magnet is neglisibly small so that the effect on the motion of the protons is weak. The optical signal from the scintillator is converted into the electric signal by photomultiplier tube (PMT). The detection resolution of the TOF system is determined by the rising time of the PMT signal in our case. The rize time of TOF-0°

and TOF-22.5° are 1 and 2.7 ns, respectively. The resultant energy resolution of TOF-0° and TOF-22.5° is 0.1 and 0.25 MeV at 3 MeV. The detection efficiencies of the TOF-0° and the TOF-22.5° systems were calibrated using monoenergetic proton beams from the ion accelerator at Kyoto Univ. [22].

RESULT AND DISCUSSION

We optimize the target position relative to the target normal direction to make the proton spectra exhibit higher energy. At the same time, we simultaneously observe the soft x-ray (~keV range) image of the focusing spot for the case of 7.5μm-Polyimide (Fig.2 (a)) and 5μm-copper (Fig.2 (b)). The sizes of the x-ray images of the focusing spot exhibit minimum at a position where the cutoff energy of proton spectra show maximum (x=0.0~μm). The laser energy is absorbed firstly into the electrons at the target, thus, an electron distribution should be reflected back to the laser spot shapes. At the same time, an X-ray image tells us the information on the electron distribution. Those electrons at the same time contribute to make the acceleration field of protons. Typical energy spectra of protons observed by the time-of-flight (TOF) spectrometers are shown in Fig.3. Panel a) shows the spectra observed by TOF-0° which is installed at target normal direction. Panel b) shows the spectra observed by TOF-22.5° which is installed at 22.5° from the target normal direction. In both panels, red, black, and blue lines show the data obtained with a 7.5μm, a 12.5μm, and a 25μm-thick Polyimide-target, respectively. All through the experiment, we observe higher maximum energy of proton spectra and higher proton flux from TOF-0° spectrometer.

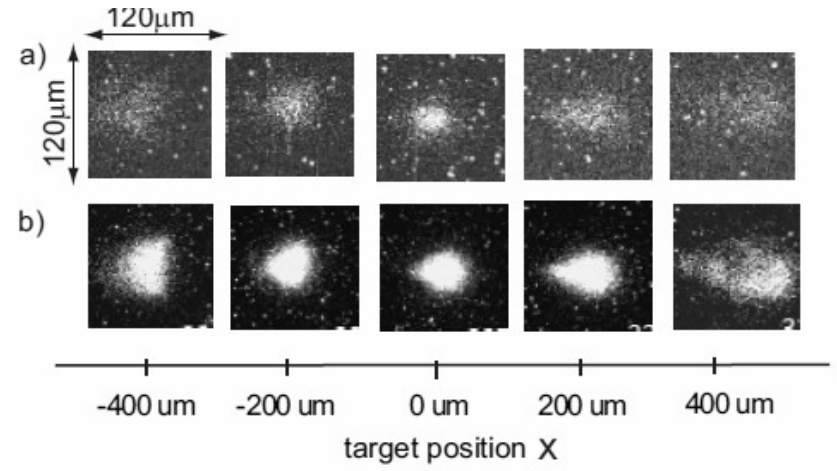

FIGURE 2. Soft x-ray (≥1 keV) images of the target front surface of a) Polyimide 7.5 μm and b) copper 5 μm targets, depending on the target position. Position 0.0 μm corresponds to the position where the proton spectra shows maximum energies of ~4 MeV. At position 0.0 μm, the plasma size seen in the x-ray images takes the minimum size. We observed brighter and smaller in size x-ray spots for the case of copper target than that of the Polyimide target.

The maximum energy of the protons observed with TOF-0° is up to 4 MeV for 7.5μm and 12.5μm-Polyimide-targets. We observe maximum energy of ~3.5 MeV for 25μm -target. We observe highest proton flux with a 7.5μm–target. We also observe small change in the maximum energy of proton and the conversion efficiency of laser energy into proton kinetic energy when we change the target thicknesses mentioned above. We investigated the maximum proton energy dependence on the duration of the ASE pedestals by changing the timing of the Pockels cell's switching time to be 1.5 ns or 3 ns before the main pulse arrival. We obtain higher energy protons with shorter duration of the ASE pedestals.

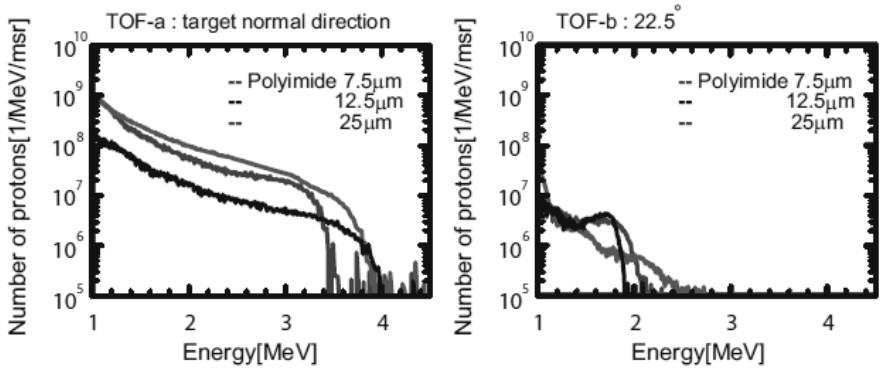

FIGURE 3. Typical energy spectra of protons observed by the time-of-flight (TOF) spectrometer. Panel a) shows the data from TOF-0° installed at target normal direction and panel b) from TOF-22.5° at 22.5°from the target normal direction. In both panels, red, black, and blue lines show the data with 7.5μm, 12.5μm, and 25μm -target, respectively.

We measure the transverse intensity profile of the proton beam with a 7.5μm -thick target at specific energy ranges, such as, >0.8 MeV, >1.8 MeV, >2.3 MeV, and >2.8 MeV by placing the CR-39 nuclear track detector (Nagase-Landauer Ltd. BARYOTRAK) installed at 82.3 mm from the target position as are shown in in Fig.4 (a),(b),(c), and (d). The CR-39 detectors are covered with Mylar or Al range filters whose thicknesses are determined for detecting the protons in each energy range as is shown in Fig.4, where the darker region corresponds to the higher intensity region. Each image in Fig.4 is recorded by single shot. The angular divergence of the beam is determined by the single-track-counting of the etch-pits on the CR-39 images for the protons whose energies are >1.8 MeV, >2.3 MeV, and >2.8 MeV, respectively. In Fig.4(f), the angular distribution of the protons with energies of >1.8 MeV is shown. The data points except the one at an angle of 0° are deduced from the single-track-counting on the CR-39 detector. However, the data points at an angle of 0° is deduced by integrating the data taken by the TOF-0° spectrometer, because the number of etch-pits at the central part of the patterns is too many to count the accurate number of protons. By fitting with the gaussian for the transverse proton intensity distribution, we determine the divergence angle to be ~30 degree ($1/e^2$) for the protons with energies of >1.8 MeV, >2.3 MeV, and >2.8 MeV. For the protons with energies of >0.8 MeV, the image recorded on the CR-39 detectors shows annular pattern. This

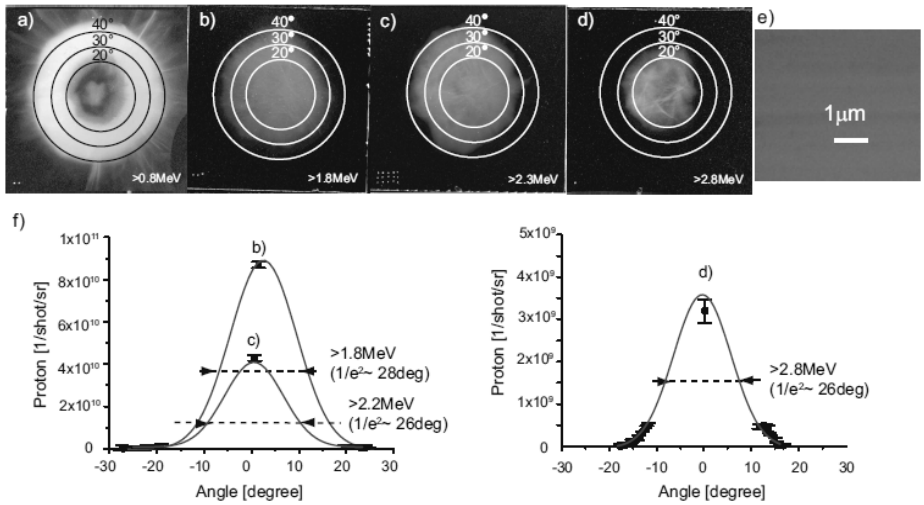

FIGURE 4. Angular distribution of the protons produced using the 7.5 μm -Polyimide target. Panels show the proton patterns on the CR-39 track detector with energies a) >0.8 MeV, b) >1.8 MeV, c) >2.3 MeV, and d) >2.8 MeV, respectively. Brighter region in these panels contain etch-pits of the protons. Protons with higher energies show the narrower angular distributions. Panel e) shows the smooth surface profile of the Polyimide target taken by an electron microscope. Panel f) shows the angular distribution of the protons with energy of >1.8 MeV obtained by the single-track counting. We fitted the measured distribution with a Gaussian yeilding the half divergence angle of ~14° at the $1/e^2$ magnitude. Because the region near the center is filled with too much etch-pits, we extract the data point at the center by accumulating TOF spectrum.

pattern is coming from the saturation of the CR-39 detectors at the center of the beam pattern [23]. It is difficult to carry out the single-track-counting from every place in the image. We, therefore, determine only the low intensity part of the beam with energies of >0.8 MeV to be >40°. The total numbers of protons are 1×10^{12}, 2×10^{10}, 9×10^{9}, and 3×10^{9} in the proton energies of >0.8 MeV, >1.8 MeV, >2.3 MeV, and >2.8 MeV, respectively. The conversion efficiencies from laser energy into the kinetic energies of protons are determined to be up to ~3%, ~0.4%, ~0.3%, and ~0.1%, in the energy ranges of >0.8 MeV, >1.8 MeV, >2.3 MeV, and >2.8 MeV, respectively. By using a relatively simplified experimental setup in combination with the 100 TW class laser system, such a high conversion efficiency from laser energy into the kinetic energies of protons has been achieved.

The obtained proton beam is shown to be emitted in a laminar fashion. The quality of the beam is good enough to be used for the proton radiography. Figure 5 shows the experimental setup used for obtaining the proton radiography of the copper mesh. We use CR-39 detectors covered with Al filters to detect copper mesh image of the proton radiography. The energy band of the protons for the radiography is >2.3 MeV. The mesh used is originally the test pattern of an electron microscope i.e., H7 Reference Pattern, 400 Mesh fabricated by Maxtaform Co. Ltd., whose pitch and bar width are 63μm and 12μm, respectively. The actual pitch is measured to be 62.5±0.6μm with an optical microscope. The thickness of the mesh is 12μm, which is smaller than the

stopping range of 2.3 MeV protons in the copper (=22.5μm). We obtain clear image of the copper mesh as is shown in Fig.6. In order to determine the proton beam quality in terms of transverse emittance, we measure the magnification of the mesh image from the experimental data which are obtained by changing the distance between the target and the detector (L), such as 82.3±0.5, 168.3±0.5, and 254.3±0.5 mm. The distance between the target and the mesh is fixed to d = 7.5±0.5 mm. The fact that the beam which is emitted in laminar fashion from the actual source position on the target can be explained that the beam is emitted from the virtual source with finite size which is located at distance x behind the target (Fig.5) [3]. The virtual source position x is determined by the experimental data and the expression, $M_{exp} = (x+d)/(x+L)$. We, therefore, can determine the position of the virtual source position to be 0.4~0.5 mm. If we assume that the virtual source size can be estimated with the technique similar to that used in geometrical ray optics [26, 27], where the scattering of a proton at the edge of the bars in the mesh-structure is ignored, the virtual source size can be detemined to be ~20μm from the spatial resolution of the radiography. As a result, the transeverse emittance is detemined to be ~0.03 π mm mrad.

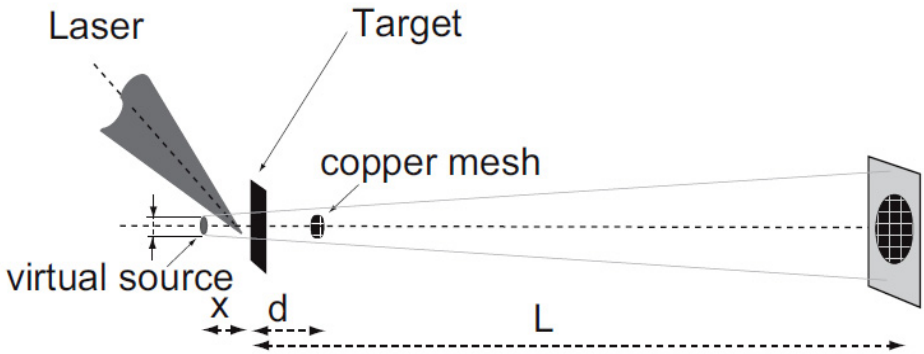

FIGURE 5. Angular distribution of the protons produced using the 7.5 μm -Polyimide target. Panels show the proton patterns on the CR-39 track detector with energies a) >0.8 MeV, b) >1.8 MeV, c) >2.3 MeV, and d) >2.8 MeV, respectively. Brighter region in these panels contain etch-pits of the protons. Protons with higher energies show the narrower angular distributions. Panel e) shows the angular distribution of the protons with energy of >2.8 MeV obtained by the single-track counting. We fitted the measured distribution with a Gaussian yielding the half divergence angle of ~14° at the $1/e^2$ magnitude. Because the region near center is filled with too much etch-pits, we extract the data point at the center by accumulating the TOF spectrum.

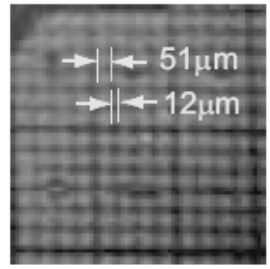

FIGURE 6. A Cu mesh is backlighted in a single shot with protons whose energies are > 2.3 MeV. whiter regions in the image correspond to the etch pits of the proton bombardments. On the other hand the blackened parts are shadow of the mesh in which less proton bombardment is found. A magnified section of the image for the case of magnification of ~20 is shown. The scale is in object-plane units. The letter "O" is visible at the lower-left corner on the image. The scales of the bars and holes in the mesh are 12 μm and 51 μm.

We performed 2-Dimensional Hydro-Dynamic (hereafter 2D HD) simulation of the evolution of the 7.5μm -Polyimide-target irradiated by an ASE pedestal and a pre-pulse using the PINOCO code [28].

The pre-pulse and the ASE pedestals are incident on the target at right angles. They are in the Gaussian distributions in the transverse direction with the FWHM waists of 10μm. The measured condition is shown with the solid line in Fig.7 (hereafter condition-1). The ASE pedestals change their intensity at the time of the switching time of the Pockels cell. The pre-pulse whose intensity and the duration are 3×10^{14} and 34 fs irradiates the target 4.2ns before the main pulse arrival, followed by the ASE pedestals whose intensity (duration) are 3×10^{9} (continues from 4.2 ns to 0.8 ns before the main pulse) and 1.2×10^{12} (continues from 0.8 ns to just before the main pulse arrival). The dotted line in Fig.7 shows the pre-pulse condition with ASE pedestals with lower intensity (hereafter condition-2). The electron density profile just before the main pulse arrival derived from 2D HD simulation is shown in Fig. 8(b) and (c) for condition-1 and condition-2. Figure 8 (a) shows the typical plasma image from an interferometer with the 800-nm probe 50ps before the main-pulse arrival. We observe no clear fringe shifts n both sides of the target surfaces. The effective pre-pulse condition might be related not to condition-1 but condition-2. One possible explanation is that the effective absorption of the laser light into Polyimide target is lower than expected because Polyimide target is transparent to 800 nm wavelength. In our acceleration regime, the target rear surface might remain in the solid density and stay at the initial position.

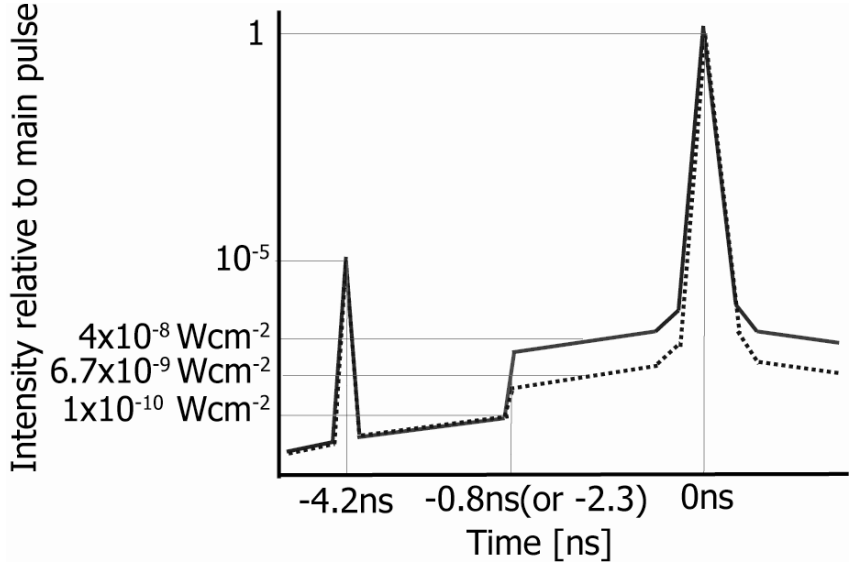

FIGURE 7. Condition of the pre-pulse which is the leakage from the regenerative amplifier and ASE pedestals. The ASE pedestals change their intensity at the time of the switching time of the Pockels cell (-0.8ns). The measured condition is shown with the solid line (hereafter condition-1), which is the case for the copper target. The effective condition (hereafter condition-2) is shown with the dotted-line, which is the case for the Polyimide targets.

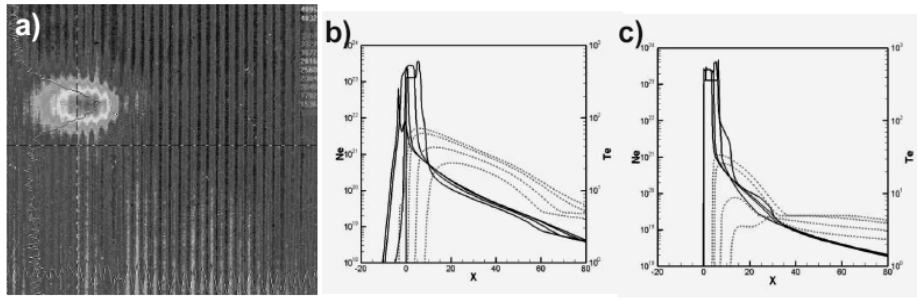

FIGURE 8. (a)Typical plasma image from interferometer with the 800-nm probe 50ps before the main-pulse arrival for the 7.5μm-Polyimide target. (b)The electron density profiles at initial time (rectangular profile) and just before the main pulse arrival with the ASE condition-1. (c) Same as (b) but with ASE condition-2.

Figure 9 (a)-(d) shows the intensity profile of the proton beam from 5μm-copper target. It is clear that many lines in the vertical direction are seen in the intensity profile (Fig.9 (b)-(d)). The intensity profile is saturated again, in the lowest energy range (Fig.9 (a)). The structures seen in Fig.9 (b)-(d) are considered to be transferred ones from the surface structures of the copper target [4, 29].

The plasma image and the electron density profiles from the 2D HD simulation just before the main pulse arrival is shown in Fig.10 (a) and (b). The ASE condition-1 was assumed for the 5μm-copper target. We observed no fringe shifts on both sides of the target. The simulation results tell us that the rear side of the target remains in the solid density and stays at the initial position. These are the evidences which strongly support the fact that the structures at the rear side of the target is transferred to the intensity profile of the proton beam. Figure 9 (e) shows the close look up of the 5μm-copper target surface taken with an electron microscope. There exist many grooves in the vertical direction which are coming from manufacturing process of the copper tape itself. The grooves are ~2 μm in pitches and ≤1μm in depths. We observe ~8-10 lines within the intensity profile of the beam. From this information we can restrict the size of the proton emitting region to be ~20 μm. It is about the same order but somewhat larger than the size of the focal spot of ~17 μm ($1/e^2$ diameter).

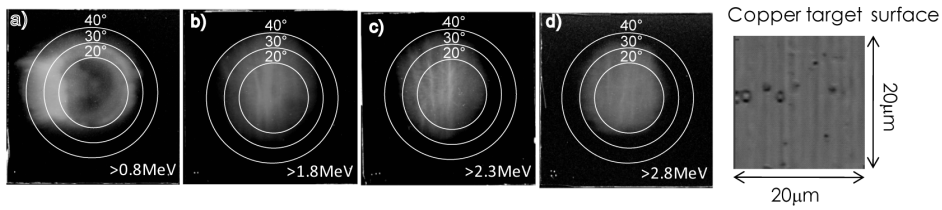

FIGURE 9. Intensity profiles of the proton beam from a 5μm-thick copper target with proton energies a) >0.8 MeV, b) >1.8 MeV, c) >2.3 MeV, and d) >2.8 MeV, respectively. e) Microscopic observation of 5 μm -copper tape target. Many grooves other than spots are on the surface of the target which are due to the manufacturing process of the target itself. Grooves are ~2 μm in periods and ≤1 μm in depths.

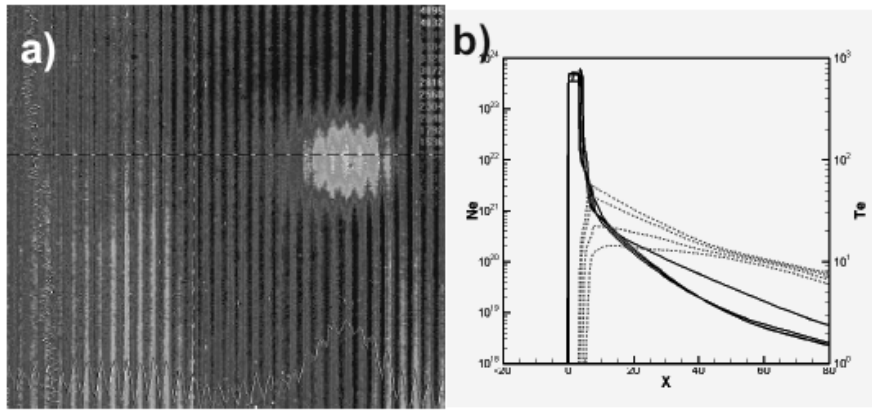

FIGURE 10. (a)Typical plasma image from an interferometer with the 800-nm probe 50ps before the main-pulse arrival for the 5μm-copper target. (b)The electron density profiles at initial time (rectangular profile) and just before the main pulse arrival with the ASE condition-1.

SUMMARY

We have demonstrated the high-flux proton generation with energy of up to 4 MeV with the conversion efficiency of ~3%, using 1.7 J, 34 fs, $3x10^{19}$ Wcm^{-2} laser pulses repetitively irradiating on the relatively thick 7.5, 12.5 and 25 μm-Polyimide targets, by keeping the ASE levels not to blow out the target rear surfaces.

ACKNOWLEDGMENTS

We would like to thank Drs. T. Tajima, T. Kimura, S. Kawanishi, M. Nishikino, and M.P. Pirozhkova for their support, suggestions, and useful discussions. This work was partly supported by the Ministry of Education, Culture, Sports, Science and Technology of JAPAN and Japan Science and Technology Agency (The three-country joint research of Japan-Korea-China). This work partly supported by Special Coordination Funds for Promoting Science and Technology (SCF) commissioned by the Ministry of Education, Culture, Sports, Science and Technology(MEXT) of Japan. This work was partially supported by the Korea Foundation for International Cooperation of Science & Technology(MOST) in 2006. (No. M60404000008-06B0400-00810), and also by the Ministry of Commerce, Industry and Energy of Korea through the Industrial Technology Infrastructure Building Program.

REFERENCES

1. G. Mourou, T. Tajima, S.V. Bulanov: *Rev. Mod. Phys.* 78, 309 (2006).
2. M. Borghesi, J. Fuchs, S. V. Bulanov, A. J. Mackinnon, P. Patel. M. Roth: *Fusion Science and Technology 49*, 412 (2006).
3. M. Borghesi, A. J. Mackinnon, D. H. Campbell, D. G.Hicks, S. Kar, P. K. Patel, D. Price, L. Romagnani, A. Schiavi, O. Willi:*Phys. Rev. Lett*., 92, 055003 (2004)
4. T. E. Cowan, J. Fuchs, H. Ruhl, A. Kemp, P. Audebert, M.Roth, R. Stephens, I. Barton, A. Blazevic, E. Brambrink, J. Cobble, J. Fernandez, J.-C. Gauthier, M. Geissel, M. Hegelich, J. Kaae, S. Karsch, G. P. Le Sage, S. Letzring, M. Manclossi, S. Meyroneinc, A. Newkirk, H. Pepin, N. Renard-LeGalloudec: *Phys. Rev. Lett*., 92, 204801 (2005)
5. M.Nishiuchi, H.~Daido, A.~Sagisaka, K.~Ogura, S.~Orimo, K.~Kado, A.~Yogo, M.~Mori, Y.~Hayashi, S.~Bulanov, A.~Fukumi, Z.~Li, A.~Noda, and S.~Nakamura: *Appl. Phys. B.,* 87, 615 (2007)
6. K.~Kurshelnick, E.L.~Clark, R.Allott, F.N.Beg, C.N.Danson, A.Machacek, V.Malka, Z.Najmudin, D.Neely, P.A.Norreys, M.R.Salvati, M.I.K.Santala, M.Tatarakis, I.Watt, M.Zepf, A.E.Dangor: *IEEE Trans. Plasma Sci.* 28, 1184 (2000)
7. D.Habs, G.Pretzler, A.Pukhov, J. Meyer-twer-vehn, Prog. Part. *Nucl. Phys.* 46, 375 (2001)
8. I. Spencer, K. W. D. Ledingham, R. P. Singhal, T. McCanny, P. McKenna, E. L. Clark, K. Krushelnick, M. Zepf, F. N. Beg, M. Tatarakis, A. E. Dangor, P. A. Norreys, R. J. Clarke, R. M. Allott and I. N. Ross: *Nucl. Instrum, Methods Phys. Res., Sect. B* 183, 449 (2001).
9. M. Borghesi, A. Schiavi, D. H. Campbell, M. G. Haines, O. Willi, A. J. MacKinnon, L. A. Gizzi, M. Galimberti, R. J. Clarke, H. Ruhl: *Plasma Phys. Controlled Fusion 43*, A267 (2001).
10. F.B. Boody, R. Hoepfl, H. Hora: *Laser Part. Beams,* 14, 443 (1996).
11. M. I. K. Santala, M. Zepf, F. N. Beg, E. L. Clark, A. E. Dangor, K. Krushelnick, M. Tatarakis, I. Watts, K. W. D. Ledingham, T. McCanny, I. Spencer, A. C. Machacek, R. Allott, R. J. Clarke, P. A. Norreys: *Appl. Phys. Lett.* 78, 19 (2001)
12. K. Nemoto, A. Maksimchuk, S. Banerjee, K. Flippo, G. Mourou, D. Umstadter, V. Yu. Bychenkov: *Appl. Phys. Lett.* 78, 595 (2001)
13. S. C. Wilks, A. B. Langdon, T. E. Cowan, M. Roth, M. Singh, S. Hatchett, M. H. Key, D. Pennington, A. MacKinnon, and R. A. Snavely: *Phys. Plasmas 8*, 542 (2001)
14. R. A. Snavely, M. H. Key, S. P. Hatchett, T. E. Cowan, M. Roth, T. W. Phillips, M. A. Stoyer, E. A. Henry, T. C. Sangster, M. S. Singh, S. C. Wilks, A. MacKinnon, A. Offenberger, D. M. Pennington, K. Yasuike, A. B. Langdon, B. F. Lasinski, J. Johnson, M. D. Perry, and E. M. Campbell: *Phys. Rev.Lett.* 85, 2945 (2000)
15. Stephen P. Hatchett, Curtis G. Brown, Thomas E. Cowan, Eugene A. Henry, Joy S. Johnson, Michael H. Key, Jeffrey A. Koch, A. Bruce Langdon, Barbara F. Lasinski, Richard W. Lee, Andrew J. Mackinnon, Deanna M. Pennington, Michael D. Perry, Thomas W. Phillips, Markus Roth, T. Craig Sangster, Mike S. Singh, Richard A. Snavely, Mark A. Stoyer, Scott C. Wilks, and Kazuhito Yasuike: *Phys. Plasmas* 7, 2076 (2000)
16. A. J. Mackinnon, Y. Sentoku, P. K. Patel, D.W. Price, S. Hatchett, M. H. Key, C. Andersen, R. Snavely, and R. R. Freeman: *Phys. Rev. Lett*. 88, 215006 (2002)
17. T. Nayuki et al., *J. Appl. Phys.* 100, 043111 (2006);
18. A. Sagisaka et al.
19. M. Kaluza, J. Schreiber, M. I. K. Santala, G. D. Tsakiris, K. Eidmann, J. Meyer-ter-Vehn, and K. J.Witte: *Phys. Rev. Lett.* 93, 045003 (2004)
20. E. Fourkal, B.Shahine, M.Ding, J.S. Li, T.Tajima, and C.-M. Ma: Med. Phys. 29, 2788 (2002)
21. T. Esirkepov, M.Yamagiwa, and T. Tajima: *Phys. Rev. Lett.* 96, 105001 (2006)
22. S. Nakamura et al., *Jpn. J. Appl. Phys*. 45, L913 (2006); A. Yogo et al., *Phys. Plasmas* 14, 043104 (2007)
23. S. Gaillard, J. Fuchs, N. Renard-LeGalloudec, and T.E. Cowan, *Phys. Rev. Lett.* 96, 249201 (2006);
24. D. Neely et al., *Appl. Phys. Lett.* 89, 021502 (2006);
25. P. Antici et al., *Phys. Plasmas.* 14, 030701 (2007);
26. A.~V.~Baez: *J. Opt. Soc. Am,* 42, 756 (1952)
27. M. R. Howells and M. A. Iarocci: *J. Opt. Soc. Am.* A3, 2171 (1986)

28. H. Nagatomo et al. *Phys. Plasmas* 14, 056303 (2007)
29. H.Ruhl, T.Cowan, and J.Fuchs: *Phys. Plasmas* 11, L17 (2004)